Ultrahigh-water-content biocompatible gelatin-based hydrogels: Toughened through micro-sized dissipative morphology as an effective strategy

Materials Science & Engineering C 120 (2021) 111750

Contents lists available at ScienceDirect

Materials Science & Engineering C

journal homepage: www.elsevier.com/locate/msec

Ultrahigh-water-content biocompatible gelatin-based hydrogels: Toughened through micro-sized dissipative morphology as an effective strategy

M. Sheikhi [a], F. Rafiemanzelat [a,*], L. Moroni [b,*], M. Setayeshmehr [b,c,d]

[a] Polymer Chemistry Research Laboratory, Department of Chemistry, Isfahan 81746-73441, Islamic Republic of Iran
[b] MERLN Institute for Technology Inspired Regenerative Medicine, Complex Tissue Regeneration Department, Maastricht University, Universiteitssingel 40, 6229ER Maastricht, the Netherlands
[c] Department of Biomaterials, Tissue Engineering and Nanotechnology, School of Advanced Technologies in Medicine, Isfahan University of Medical Sciences, Isfahan, Iran
[d] Department of Tissue Engineering & Regenerative Medicine, Faculty of Advanced Technologies in Medicine, Iran University of Medical Sciences (IUMS), Tehran, Iran

ARTICLE INFO

Keywords:
Supramolecular interactions
Microgels
Gelatin
Biomaterials
Dissipative morphology

ABSTRACT

Fabrication of simultaneously robust and superabsorbent gelatin-based hydrogels for biomedical applications still remains a challenge due to lack of locally dissipative points in the presence of large water content. Here, we apply a synthesis strategy through which water absorbency and energy dissipative points are separated, and toughening mechanism is active closely at the crack tip. For this, gelatin-based microgels (GeMs) were synthesized in a way that concentrated supramolecular interactions were present to increase the energy necessary to propagate a macroscopic crack. The microgels were interlocked to each other via both temporary hydrophobic associations and permanent covalent crosslinks, in which the sacrificial binds sustained the toughness due to the mobility of the junction zones and particles sliding. However, chemical crosslinking points preserved the integrity and fast recoverability of the hydrogel. Hysteresis increased strongly with increasing supramolecular interactions within the network. The prepared hydrogels showed energy loss and swelling ratio up to 3440 J. m^{-3} and 830%, respectively, which was not achievable with conventional network fabrication methods. The microgels were also assessed for their in vivo biocompatibility in a rat subcutaneous pocket assay. Results of hematoxylin and eosin (H&E) staining demonstrated regeneration of the tissue around the scaffolds without incorporation of growth factors. Also, vascularization within the scaffolds was observed after 4 weeks implantation. These results indicate that our strategy is a promising method to manipulate those valuable polymers, which lose their toughness and applicability with increasing their water content.

1. Introduction

Hydrogel-based matrices are a very important class of scaffolds due to the ability to tailor their characteristics to mimic those of natural tissues. [1,2]. In the context of biomaterial properties, swelling characteristic of hydrogels could result in complications in case of implants [3]. [4,5]. Recent studies highlighted the potential of these particular scaffolds to maintain in vivo cellular activity and facilitate vascularization [4,5].

Recently, hydrogels based on natural extracellular materials, such as collagen or gelatin, have gained a lot of interest in the realm of drug delivery and tissue engineering thanks to cell signaling and cell-interactive motifs present in their backbone [6–8]. The most important limitation attributed to gelatin-based hydrogels is the loss of effective toughening mechanism to sustain mechanical stress and resist fracture especially in the presence of large water content, which limits their performance in regards to biomedical applications [9–11].

Many strategies have been applied to enhance hydrogels' mechanical properties, including tensile strength, compressive strength and toughness. These strategies are based on the fabrication of tough gelatin-based hydrogels through self-crosslinking [12–14], developing interpenetrating *polymer* networks (IPN)s with polysaccharides such as

* Corresponding authors at: Biomaterials, Nanotechnology and Tissue Engineering Group, Department of Advanced Medical Technology, Isfahan University of Medical Sciences, Isfahan 817467-3461, Islamic Republic of Iran.
E-mail addresses: frafiemanzelat@chem.ui.ac.ir (F. Rafiemanzelat), l.moroni@maastrichtuniversity.nl (L. Moroni).

https://doi.org/10.1016/j.msec.2020.111750
Received 27 August 2020; Received in revised form 10 November 2020; Accepted 22 November 2020
Available online 27 November 2020

alginate [15,16], chitosan [17], hyaluronan [18], alginate/fibrinogen [19] or doping nanomaterials [20,21]. All these strategies share a common theme, i.e. introducing energy dissipation mechanisms into the polymer network while maintaining macroscopic integrity. However, the hydrogel is commonly engineered so that water absorption and dissipation mechanisms take place at the common zones. Thus, the large water contents impair molecular interactions, following disruption in their dissipation capability required to prevent crack propagation [22–25]. Therefore, designing a strategy to enhance the toughening mechanism of hydrogels is still considered as an open challenge in biomaterials science.

Supramolecular hydrogels show toughness due to breakage and reformation of junction points upon loading and unloading, respectively. In this context, the most important factors in the performance of these interactions are the amplitude and fraction (the concentration and number of mentioned interactions) of supramolecular interactions. Typically, macroscopic fracture originates from the growth of small defects (e.g. cracks) due to material damage induced by the amplified local stress field surrounding the defects [23,26–28]. Thus, the introduction of high concentration of supramolecular interactions in micro-sized separated domains as toughening mechanism may effectively render energy dissipation near the crack point and overcome efficiently crack propagation. Additionally, separation of energy dissipative and water absorbent sectors would be efficient to prevent the negative effect of large water content on dissipative interactions.

we introduce concentrated dissipative points via specific micro-sized morphology, through which the applied stress is dissipated quickly at the point. It is expected that the presence of supramolecular interactions located in excess at the micro-sized points could induce dissipation of crack energy within the junction zones.

For this purpose, we prepared modified gelatin microgels (GeMs), in which the particles possess internal H-bondings and superficial hydrophobic poly (glycidyl methacrylate) segments (PGMAs), which contribute to damping of the applied energy. In addition, the GeMs will be chemically interlinked to each other after the reaction of newly synthesized amine-terminated linkers with epoxy groups of superficial PGMAs. At the same time, this method ensures super-absorbency, because the majority of toughening mechanisms are active on the microgel particles whereas the internal structure of microgels is responsible for water absorbency.

2. Experimental section

2.1. Materials

75 Bloom gelatin powder (bovine gelatin) was obtained from Merck (Germany). The emulsifier used was the reagent-grade span 60 (non-ionic emulsifier, Sorbitan Monostearate 60, provided by Sigma-Aldrich). Ammonium peroxodisulfate (APS, Merck) was used as water soluble initiator without further purification. Glycidyl methacrylate and acrylic acid (AAc) was also obtained from Merck and used without purification.

2.2. Modification of gelatin

Glycidylated gelatin (GM-gelatin) was prepared by the reaction of gelatin with glycidyl methacrylate. In detail, 6 g gelatin was dissolved in 50mL phosphate buffer (pH 7.5, 0.2 M) at 50 °*C* for 0.5 h. Then, 0.5 mL glycidyl methacrylate (1.50mmol) was added dropwise while vigorously stirring for 8 h. The modification of gelatin was proved by FT-IR spectroscopy (FT-IR 0066 Spectrophotometer, Jasco, A thin film of polymer solution was casted on KBr plate).

The degree of substitution (DS) is described as the fraction of amine groups that are modified. This was accomplished by the following ninhydrin assay procedures. Briefly, the reaction of ninhydrin and free amine groups at 100 °*C* led to a purple compound. The optical absorbance of the resulting solution was measured at 570 nm using a UV–Vis spectrophotometer (500 UV–Vis-NIR spectrophotometer, Cary). The number of free amine groups in the GM-gelatin, which reacted with ninhydrin, is proportional to the optical absorbance of the solution. The degree of substitution can be calculated by the Eq. (1) [29]:

$$DS = \frac{(NH_2)_g - (NH_2)_{mg}}{(NH_2)_g} \times 100 \quad (1)$$

where $(NH_2)_g$ and $(NH_2)_{mg}$ are the optical absorbance of gelatin and modified gelatin, respectively. The measurement was repeated four times to calculate the average and standard deviation.

2.3. Synthesis of gelatin microgels (GeMs)

Batch inverse emulsion polymerizations of GM-gelatin macromonomers were carried out at 65°*C*. The aqueous phase containing 20 g of GM-gelatin solution previously prepared, AAc, 0.024 g APS and 0.28 g Span 60 were added dropwise into the reactor, which previously contained the oil phase including GMA in 50 mL toluene, under vigorous stirring (3200 rpm). The mixture stirred for 15 min at 3200 rpm to obtain a homogeneous milky solution. The amount of ingredients varied as shown in Table 1. When all the ingredients were added, the reaction temperature achieved the desired setting of 65 °*C* and reaction processed for 3 h. The dispersion was purified by dialysis against distilled water for 4 days and then stored in closed tubes for characterization and further utilization. The dispersed synthesized GeMs in water were spread on a glass and imaged by light microscopy (TSI, TG-5-3). The particle size of dispersed GeMs in water was determined by the dynamic light scattering (Bettersizer 2600, Bettersize) method. Transmission electron microscopy (TEM, JEM-2100F) was used to observe the presence of PGMAs grafted on microgels.

Determination of the epoxide value was carried out according to the reported procedure with minor modification [30]. Briefly, the back-titration method was used to determine the epoxide value; the epoxide value was calculated according to Eq. (2):

$$EV = \frac{(V_0 - (V'' - V')) \times N}{W \times 10} \quad (2)$$

where, V_0 is the volume (mL) of NaOH aqueous solution consumed by hydrochloric acid present in the solution with no dissolved sample. (V″-V′) = V, which is the difference between the volumes (mL) of NaOH aqueous solution consumed by hydrochloric acid present in the solution with dispersed microgels samples with (V'') and without (Gel_0) grafted PGMAs chains (V′). N (mol/L) is the concentration of NaOH standard aqueous solution and W is the mass (g) of the solid fraction of the utilized dispersion. The measurements were repeated four times to calculate the average and standard deviation.

2.4. The sol-gel transition study and determination of limited water content (LWC)

The synthesized microgels were stepwise dehydrated under vacuum

Table 1
Initial composition used in the preparation of the GeMs.*

Specimen	Aqueous phase			Organic phase		Particle size (μm)
	GM-gelatin (gr)	AAc (mL)	APS (gr)	GMA (mL)	Span60 (gr)	
Gel_I	20	0.3	0.024	0.5	0.28	23
Gel_{II}	20	0.6	0.024	0.5	0.28	49
Gel_{III}	20	0.6	0.024	0.8	0.28	69
Gel_0	20	0.6	0.024	0	0.28	35

* 0.25 mL of linker solution with 6 % w/v concentration was used for chemical crosslinking of GeMs.

to predominate supramolecular interactions and achieve sol-gel transition. GeMs were exposed to reduce 0.5 mL of the total volume then set aside at room temperature for 40 min to monitor their physical state. This step was repeated for each specimen until their transitions to gel state. This transition is attributed to predomination of supramolecular interactions hydrophobic interactions. Results of attenuated total reflection Fourier transform infrared spectroscopy ATR-FTIR (ATR-PR0410-M, Jasco) were used to investigate the formation of supramolecular interactions. In addition, heating-cooling temperature sweep rheometry (MCR 302, Anton Paar) was applied to study rheometrical properties of the formed physical gels. In order to determine LWC, defined as maximum water content in which the supramolecular interactions predominate, the formed gels were dried completely and weighed. The loss mass was considered as the LWC. The measurement was repeated four times for each specimen to calculate the average and standard deviation.

2.5. Synthesis of amine-terminated oligo (urethane) and oligo (amide) linkers (AUX/AAX)

Poly (ethylene glycol) (PEG), molecular weight as supplied = 400 g/mol, was dried under vacuum at 120 °C for 1 h. In a two-necked 25 mL flask, 0.0025 mol (1 g) PEG 400 was dissolved at 40 °C in 8 mL previously distilled dimethyl formamide (DMF) under N_2 with gentle stirring. Isophorone diisocyanate (0.0053 mol, 1.12 mL) was then added to the solution and the temperature was raised stepwise to 50, 60, and 70 °C with intervals of 30 min for each step. Finally, the temperature reached to 75 °C and the reaction progressed 2.5 h at this temperature. 1 mL of solvent was added to the reactor every 30 min to preserve solution homogeneity. The resulting product was poured into 100mL hot water and filtered after 15 min stirring. The white precipitate was collected and rinsed three times with water. The obtained AUX was dried under vacuum at 60 °C and then characterized by FT-IR and NMR spectroscopy (Bruker Avance 500, 400 MHz). The same procedure was applied for the synthesis of AAX with the difference that PEG was replaced with previously dried sebacic acid without any changes in molar ratios.

2.6. Chemical interlocking of GeMs

In order to fabricate chemical crosslinked hydrogel, 2 g GeMs cluster (physical gel) was heated and mixed with 0.25 mL of AUX or AAX solution in DMF (6% *w/v*). The mixture was blended homogeneously and exposed to the temperature of 80 °*C* for 25 min. Chemically crosslinked microgels are represented as Gel $_x$/AUX and Gel $_x$/AAX, in which x shows the type of GeMs according to Table 1.

2.7. Swelling ratio

For the swelling evaluation, the samples were immersed in distilled water at room temperature for 24 h. Then, the sample weighed in wet condition (W_w) and let it to dry until any further weight loss was not observed (W_d). A swelling ratio was calculated as $100\times(W_w - W_d)/W_d$. The measurements were repeated four times to calculate the average and standard deviation.

2.8. Scanning electron microscopy (SEM) study

For SEM observation, hydrogels were lyophilized and cut in liquid nitrogen. Then, cross section of specimens were sputter-coated with gold (30 mA, 20 s) using an auto sputter-coater (Cressington 108) and then examined under a SEM (Hitachi S4700) at an accelerating voltage of 20 kV.

2.9. Biodegradability

The biodegradability of hydrogels was measured over 10 weeks to determine in-vitro the biodegradation rate. The cylindrical specimens with initial weight of 4 g (18 mm diameter and 3 cm height) was immersed in phosphate-buffered saline solution and weight loss was calculated as $(W_i - W_d)/W_i \times 100$, where W_i is dried initial weight and W_d is dried weight after incubation for a certain period.

2.10. Mechanical analysis

Cylindrical specimens (10 mm height and 18 mm diameter) with different formulations were subjected to a series of cyclic compression tests to 70% strains for five cycles at 1 mm min^{-1} by using a Santam 5567 machine. For hysteresis measurement, gel specimens were first compressed to a pre-determined maximum extension ratio and then unloaded. The dissipated energy was estimated by the area between the loading-unloading curves. The measurements were repeated four times for each specimen to calculate the average and standard deviation.

2.11. RMS study

For rheological characterization, the hydrogels were prepared similarly by casting of corresponding mixture solutions into molds and then chopped into pieces. The analysis was performed using a stress-controlled rheometer fitted with a Peltier stage. Examination was performed by oscillatory frequency sweeps (1–100Hz, 0.5% strain, 37 °C) to record the data of storage (G') and loss moduli (G").

2.12. Cell viability

An ideal scaffold should not yield adverse reactions or release toxic products. The 3-(4, 5-Dimethyl-2-thiazolyl)-2, 5-diphenyl-2H-tetrazolium bromide (MTT, Sigma) assay is generally known as a routine technique for evaluating the cell toxicity of biomaterials. The human adipose-derived mesenchymal stromal cells (ASCs) were resuspended in culture media (cell density, 1×10^7 cells/mL) and seeded onto scaffolds (1×10^4 cells/scaffold) by pipetting. The viability of the ASCs was analyzed by MTT assay at day 1, 3, and 7 of the culture. The viability for each time point was calculated via this formulation: [(mean value of OD of the sample) - (mean value of OD of the blank) / [(mean value of OD of the control) - (mean value of OD of the blank)].

Cell viability was also evaluated via staining with 4′,6-diamidino-2-phenylindole (DAPI, Sigma Aldrich). Briefly, the suspension of ASCs with a density of 5×10^3 cells was seeded on the top surface of each scaffold and were cultured in the incubator. A DAPI working solution (1 mg/mL) was prepared in PBS, and the cell medium was aspirated and washed three times using PBS, followed by fixing for 20 min in 2.5% formaldehyde solution. The fixative was then aspirated, the hydrogels were rinsed three times in PBS, and then incubated in DAPI solution 1 min at room temperature. Consequently, the DAPI solution was aspirated and the hydrogels were rinsed three times in PBS. To visualize the stained images, a fluorescence microscope (Nikon 80i) was used. In order to enhance image quality, Adobe Photoshop CC 2015 software was used to remove the undesired background occurred during imaging. For this, a black layer was applied on the as-obtained image and the cells figure was separated from the original image and exhibited on the black layer at their original positions and shapes. Generally, only background was removed and cell numbers and shapes were remained intact.

2.13. In vivo study

In vivo biocompatibility of the scaffolds was achieved by implantation of the scaffolds into rats. The Institutional Ethics Committee of Iran University of Medical Sciences approved informed consent and the study. Beforehand, all of the rats were isolated for a week by free access to food and water, without giving any antibiotics. The animals were housed in a controlled temperature of 24 °C, and on a 12 h light–dark cycle. For implantation of the scaffolds, rats were anaesthetized upon

surgery. Slight skin incision was created at the dorsum of the rats. A scaffold was implanted into the subcutaneous pocket of each rat. The subsequent in vivo scaffolds were harvested at 4 weeks post implantation. At sacrifice time, all constructs were harvested from the rats and processed for histological analysis. The scaffolds were removed and immediately fixed in 10% neutral buffered formalin. Scaffolds were processed by graded ethanol series before cleared by xylene. Then, the samples were embedded in paraffin and cut into 6 μm slices. Xylene-cleared sections were stained using different histological staining, Hematoxylin and Eosin (H&E), Masson's trichrome, and Toluidine blue, rinsed with distilled water, dehydrated, cleared and mounted on microscope slides.

3. Results and discussion

3.1. Characterization of GM-gelatin

Modified gelation (GM-gelatin) was synthesized by nucleophilic ring opening of glycidyl methacrylate (GMA). Partial modification of the primary amine side groups of gelatin by using GMA makes it radically polymerizable and inserts extra pendent hydroxyl groups (Fig. 1(a)). The successful modification of gelatin was verified by FT-IR spectroscopy. The appearance of the signal at 1656 cm^{-1} and widened band near 3427 cm^{-1} represents C═C and hydroxyl functions stretch vibrations of the introduced glycidyl methacrylate, respectively (Fig. 1(b)).

The degree of substitution (DS) for gelatin can be adjusted by varying the reaction time and/or the amount of GMA present in the initial reaction mixture. As longer reaction time would result in undesirable self-polymerization of vinyl groups, we used different molar ratios of GMA to achieve a relation between the followed procedure and the desired DS. In this study, the free amine groups of gelatin B were quantitatively measured by the ninhydrin assay [29]. According to the calibration curve, the amount of free amine groups in the unreacted gelatin was 0.059 mmol g^{-1}. Upon this value, different amount of GMA from 0.2 to 1.0 mL gave a 1:3 to 1:9 M excess of GMA with respect to the free amine groups of the gelatin. As illustrated in Fig. S1(c), 80% DS for gelatin was obtained at about 9-fold molar mass of GMA through our reaction method. However, higher concentration of other reagents i.e. methacrylic anhydride has been required to achieve higher degrees of vinyl substitution [29,31,32]. This is attributed to the high affinity of oxirane ring for nucleophilic attack and subsequent ring opening. In the subsequent synthesis of microgels, gelatin with 69% DS was applied instead of 80% DS, since the formation of higher irreversible crosslink density may induce rigidity and weakens the potential of formation and breakage of H-bondings for energy dissipation mechanism.

3.2. Synthesis and characterization of GeMs with concentrated supramolecular interactions

In order to improve the toughening mechanism, gelatin was modified with GMA to introduce vinyl and extra hydroxyl groups on the gelatin backbone (GM-gelatin). Next, GeMs were prepared by crosslinking of

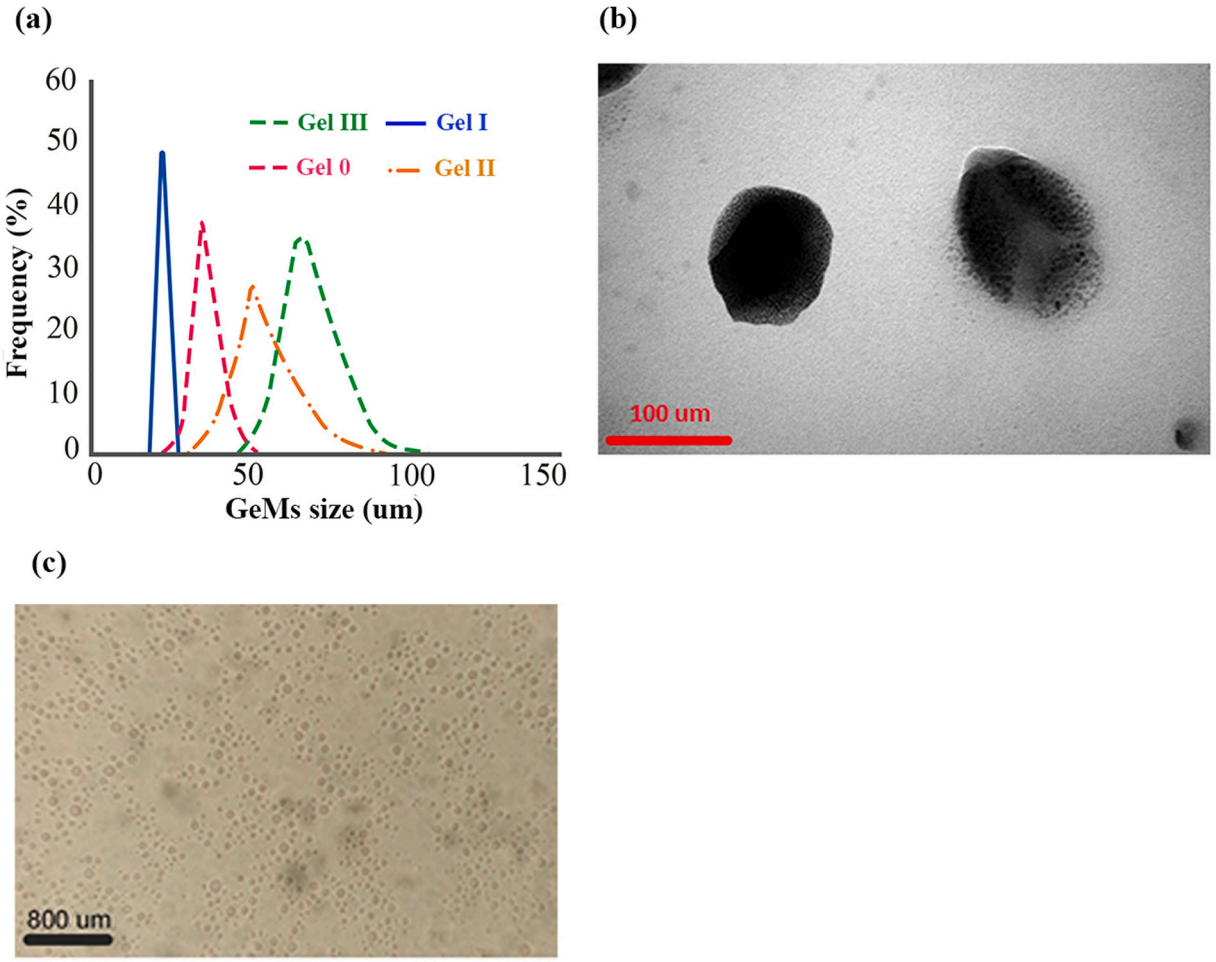

Fig. 1. (a) Particle size of GeMs prepared with different composition of aqueous and organic continuous phases. Particle of Gel_I are monodisperse colloids, however, polydisperse size was obtained for Gel_{II} and $_{III}$. (b) TEM micrographs of GeMs microgels illustrates the presence of PGMAs on the GeMs particles (Gel_{III}). (c) Optical microscopy image of Gel_{III} after purification via dialysis.

acrylic acid and C═C units of GM-gelatin via reverse emulsion radical polymerization (Fig. S2). The growing microgel particles were stabilized by steric mechanism and the feed composition varied according to Table 1.

The polymerization started inside the aqueous droplets, as the crosslinked particle cores were built up. Once the growing radical is close to the interface, it has a finite probability to cross the phase border, and the polymerization can continue from the GeMs surface in the continuous phase via the addition of GMA sequences to the GeMs. The successful formation of the PGMAs on the microgels by this type of surface diffusing initiation depends on the possibility of growing radicals to cross the phase border.

The variation of particle size for four different composition of GeMs demonstrated the incorporation of AAc monomer into the network structure of GeMs particles and functionalization of GeMs surface with PGMAs segments. As shown in Fig. 1 (a), the average size of microgels Gel_0, Gel_I, Gel_{II} and Gel_{III} was 35 μm, 23 μm, 49 μm and 69 μm, respectively. The significant difference between particles I and II at the same speed of the dispersion of components in the oil phase and the similar oil composition is attributed to the fact that larger fraction of AAc in Gel_{II} results in a more hydrophilic network formation, following more swelling behavior of Gel_{II} in DLS dispersing medium. This is confirmed by the smaller particle size of Gel_I containing lower AAc content than that of Gel_0. Further, the increased size of Gel_{III} comparing with Gel_0 and Gel_{II} at the same aqueous composition is indicative of the formation of PGMAs segments on the GeMs particles. The pile of PGMAs, due to its hydrophobic nature, accumulates in water and larger sizes are so obtained for Gel_{III}. Also, this modification was confirmed by transmission electron microscopy (Fig. 1 (b)), which proved the existing of a PGMA corona on the microgels. The obtained image from optical microscopy showed that the GeMs particles were all spherical in shape (Fig. 1 (c)).

The strategy applied here produces GeMs with two types of supramolecular interactions including internal H-bondings and superficial hydrophobic interactions of PGMAs. As illustrated in literature, the presence of water molecules impairs the formation of physical interactions between substrates following the loss of dissipation capability [50]. In this context, the concentration of such interaction points plays a critical role to overcome the undesirable effect of water molecules. In the GeMs suspension, internal H-bondings and superficial hydrophobic

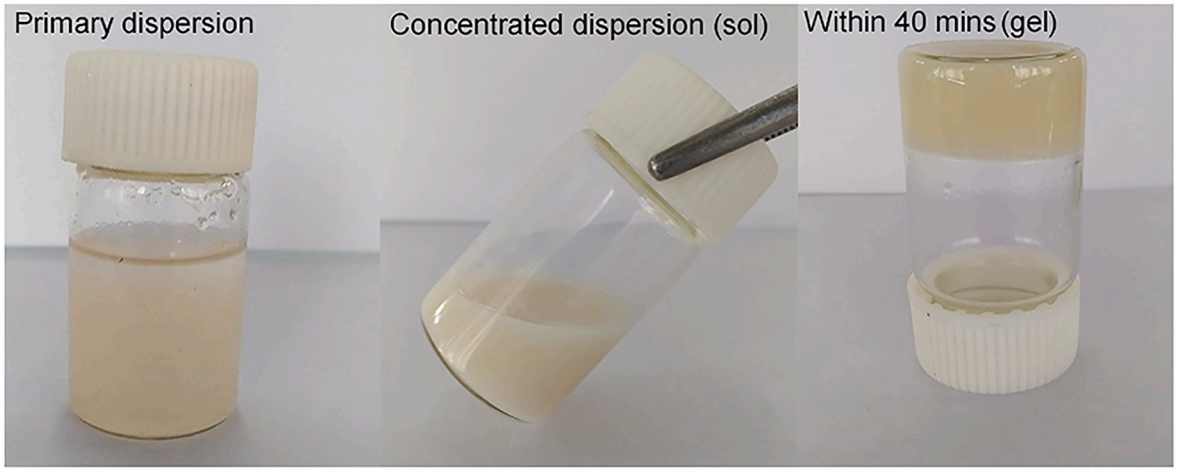

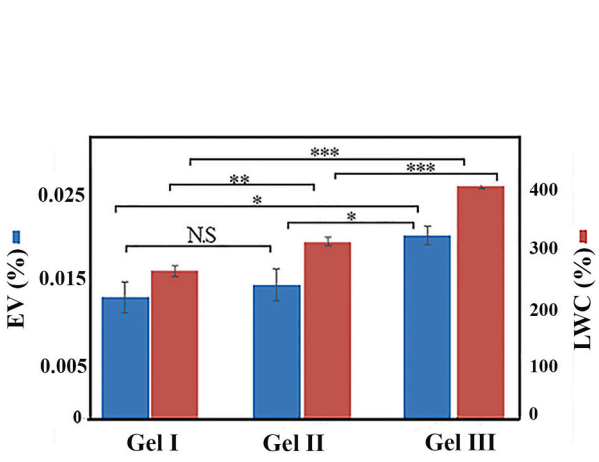

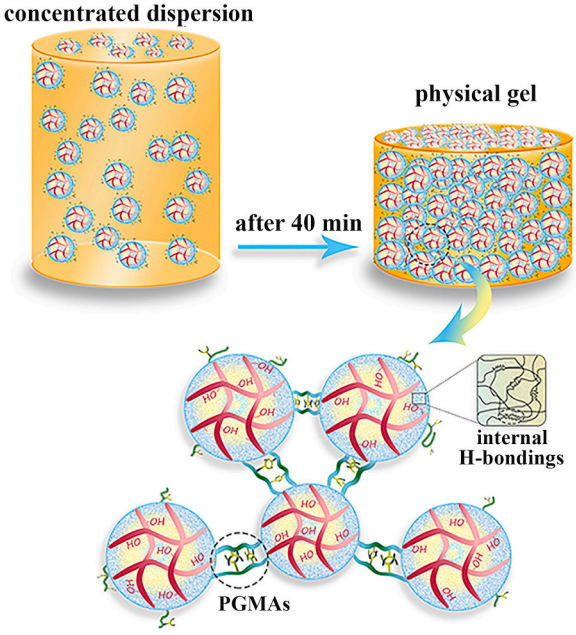

Fig. 2. (a) Sol-gel transition of GeMs particles at room temperature after prevailing physical interactions above critical concentration; (b) Limited water content (LWC) for GeMs containing AAc and PGMAs according to feed composition and EV respectively; (c) Schematic illustration for the formation and structure of physically bounded microgels through supramolecular interactions. Error bars represent means ± standard deviation for $n = 4$. N·S = Not Significant.

interactions of PGMAs appears below a specific water content (LWC) and make the GeMs to coagulate and transfer from a concentrated dispersion (sol) at room temperature to a physically bonded cluster over short time (gel) (Fig. 2 (a)). It is evident that more LWC indicates the strength of such interactions within the system. The water content of GeMs dispersion was decreased until the aforementioned supramolecular interactions predominated. As illustrated in Fig. 2 (b), LWC for the gels increased with increasing epoxy value (EV) and the content of AAc monomer utilized for microgel synthesis. EV is an indication of the GMA surface functionalization degree of GeMs. It is demonstrated that with the increase of AAc (Gel_{II}) and GMA units (Gel_{III}) in comparison with Gel_I, the supramolecular interactions are strong enough so that gelation can take place in the presence of larger amount of water (higher LWC). This confirms the influence of H-bonding and hydrophobic interactions on the formation of physical GeMs network. Also, it was observed that LWC increased of 20% (from 258 in Gel_I to 310 in Gel_{II}) when AAc was doubled, illustrating the importance of H-bonding for the formation of temporary network. However, LWC increased of 31% (from 310 in Gel_{II} to 408 in Gel_{III}) when EV increased only 1.35 fold. This observation demonstrates the superiority of superficial interactions created by PGMAs compared to internal H-bonding.

Results of FT-IR spectroscopy revealed the appearance of new bands and some shifts in the location of absorption bands for the groups involved in the aforementioned interactions. As shown in Fig. S3 (a), ester carbonyl group of PGMAs turns from a small band at 1702 cm^{-1} for sol to a more distinctive one at 1722 cm^{-1} after physical attachment of microgels for gel transition. This is attributed to the elimination of interactions between ester carbonyl groups and water after assembling of hydrophobic PGMAs segments, for which in turn the C═O absorption band shifts to higher wavenumbers. In addition, a blue shift for the gelatin amide C═O band (1639 to 1655 cm^{-1}) and a red shift for N—H (1553 to 1543) band were observed, indicating formation of new interactions inside the microgels with transition from sol to physical clustered gel. Optical microscopy images of GeMs after physical gelation of GeMs on microscope slides demonstrated that strong affinity holds the particles attached to each other (Fig. S3 (b)). Moreover, it is clear that GeMs are soft and deformable colloidal globules. In addition, the collapsed morphology of GeMs after lyophilization proves that there is a strong affinity within the GeMs causing them to collapse after removal of water (Fig. S3 (c)).

Temperature-sweep rheometry was used to ascertain the existence of supramolecular interactions, and also study the structural properties of the specimens as a function of temperature. Experimentally, the preformed gels were thermally reversible from gel state to sol-like state during the heating cycle. Gel_0 and Gel_{III} were compared to scrutinize the formation and breakage of hydrogen bonding and hydrophobic

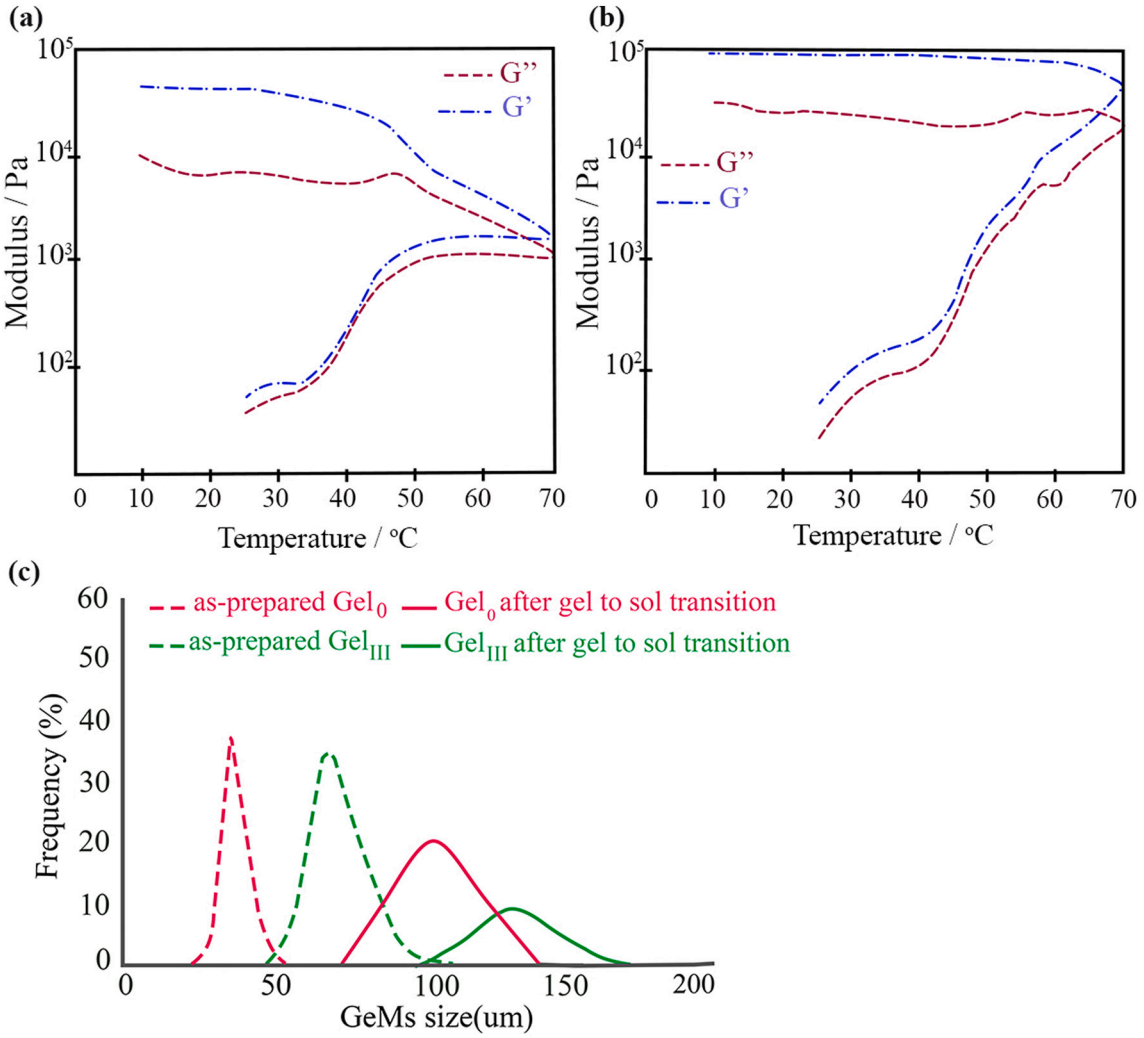

Fig. 3. (a) and (b) The rheological and structural properties of the gels Gel_0 and Gel_{III}, respectively, as a function of temperature. Inter-particle entanglements are responsible for the increase in G' as the temperature increase; (c) Comparison between the size of GeMs before and after physical gelation. Dashed and solid lines are size distribution curves for intact and secondary particles respectively.

interactions respectively during thermal cycle. It was observed that during applied heating-cooling cycle (Fig. 3 (a) and (b)), no cross over point of G"/G' curves appeared in spite of our observation for gel to sol transition at 45 °C. As the temperature increased, both G' and G" showed a nearly sharp increase, and the respective curves were close together (G'/ G" $\geq \approx 1$). $G' > G''$ indicated packing of the particles and the suspension behaved more solid like [33,34]. For Gel_0, we believe that as the temperature increases, hydrogen bonding is removed and the physical gel converts to multiple particle assemblies instead of individual particles. Due to the soft nature of microgels, some inter-particle chain entanglements are possible, which intensify with increasing the temperature. GeMs are soft and deformable particles, which reveals the fact that particles can make inter-particle entanglements. This phenomenon results in $G' > G''$ during temperature sweep. DLS results also support this idea. As illustrated in Fig. 3 (c), GeMs particles possess larger sizes after conversion from physical gel to respective sol indicating attachment of particles to each other. The same behavior was observed for Gel_{III} with the difference that G' and G" did not reach a plateau and continued to increase. This is attributed to the fact that in addition to the H-bonding assisted inter-particle chain entanglements, hydrophobic interactions significantly intensified within the multiple particle assemblies with increasing temperature. Furthermore, in comparison with Gel_{III}, the storage modulus curve of Gel_{III} was higher than that of Gel_0 over the whole temperature range, which proves the superiority of hydrophobic interactions. Another indication for the presence of supramolecular interactions is their rheological properties during cooling of the previously heated sample. During the cooling sweep, both G' and G" are high compared to initial values, which could be explained by the formation of renewed hydrogen bonds along with the assembled inter-particle entanglements. The obtained results proved the presence and performance of supramolecular interactions that we aimed to introduce in the gelatin-based microgels.

3.3. Preparation and properties of chemically linked GeMs

In cooperation with physical binding, the prepared GeMs are functionalized with epoxy groups which can be further used to chemically crosslink the particles. The role of chemical connections is to support bulk integrity and prevent network fragmentation during GeMs sliding. For chemical interlocking of GeMs, the precursor was crosslinked using newly synthesized linkers. The linkers are amine-terminated urethane (AUX) and amide (AAX) oligomers. AUX comprises long poly (ethylene glycol) (PEG) segments in the structure. AUX and AAX were synthesized via the reaction of excess amount of isophorone diisocyanate (IPDI) with PEG-400 or sebacic acid respectively (Fig. S4 (a)). FT-IR spectrum of the linkers demonstrates the formation of urethane (AUX) and amide (AAX) functional groups (Fig. S4 (b) and (c)). For AUX, the bands at 3367 cm^{-1} and 2928 cm^{-1} were a result of N—H stretching and C—H vibrations of methylene groups respectively. Appearance of the signals at 1718 cm^{-1} was due to urethane C═O vibration and 1560 cm^{-1} was attributed to–NH-C(O)- vibration. For AAX, stretching frequency of amide C═O and –NH-C(O)- groups appeared at 1637 cm^{-1} and 1544 cm^{-1} respectively. The band at 3345cm^{-1} was also assigned to hydrogen bonded N—H group. A plot of the ^{1}H NMR is shown in Fig. S4 (d) as a representative example. Number and type of hydrogen atoms are according to AUX linker structure.

$Gel_{I, II, III}$ samples were crosslinked with the same concentration of AUX based on the reaction of mutually reactive functional end group, i.e. active epoxy and amine end-group (see also graphical abstract). For this, the physical gel was heated to break the supramolecular interactions subsequently transformed to sol state and mixed with AUX. Crosslinking progressed for 20 min at high temperature. Then, the temperature decreased to room temperature so that the ruptured supramolecular interactions formed again. It should be mentioned that only a minor part of GeMs was chemically linked and the rest remained intact. AAX was just utilized for crosslinking of Gel_{III} for comparison. These types of linkers influence the mechanical and biodegradable properties of the hydrogels.

Tough hydrogels reveal remarkable dissipation of energy, which can be characterized by hysteresis. Physically and chemically crosslinked GeMs demonstrated large hysteresis. However, the structure of microgels influences dissipation properties of crosslinked networks (Fig. 4). The area enclosed by the loading and unloading curves demonstrates the energy dissipated in the cycle. The Gel_{III}/AUX hydrogel showed the largest hysteresis. However, the dissipated energies for the first cycle were 3440 J. m^{-3} for Gel $_{III}$/AUX hydrogel, 3125 J. m^{-3} for Gel $_{III}$/AAX hydrogel, 2428 J. m^{-3} for Gel $_{II}$/AUX hydrogel, 1605 J. m^{-3} for Gel $_{I}$/AUX hydrogel, and 963 J m^{-3} for Gel 0 hydrogel. The damping properties of Gel_0 was investigated up to maximum 50%, because the specimen collapsed under larger deformation [35]. Compared to conventional crosslinking methods of gelatin, the prepared gels showed larger amount of energy loss due to micro-sized dissipating morphology of fabricated 3D networks [17]. For all specimens, the dissipated energy of hydrogels decayed up to cycle 3 and remained almost stable afterward (data not shown). This morphology sustains extra bond formation/breakage phenomena, which in turn induces dissipation of crack energy within the junction zones. The entire dissipated energy during the loading/unloading cycle can be attributed to the fracture of supramolecular interaction by the Lake-Thomas mechanism [36]. It was observed that energy loss increased according to both H-bonding concentration (Gel_{II} vs. Gel_{I}) and epoxy values (Gel_{III} vs. Gel_{II}) of the GeMs (Fig. 4 (f)). This observation indicates that the origin of energy dissipation within the network corresponds to superficial non-covalent PGMAs assembled points, as well as internal H-bonds within the microgels.

A comparison of Gel_{III} with Gel_{II} with similar internal structure, but different PGMAs units, illustrates the importance of hydrophobic interactions during energy damping. It could be referred to the fact that such interactions dissociate under loading making the possibility for GeMs to slide over each other and re-associate again (Fig. S5). Subsequently, this phenomenon facilitates efficiently the dissipation of applied stress. In accordance with the data of previous rheometery analysis (Fig. 3), we observed that only 35.7% increase in EV led to 41.7% increase in dissipated energy (Gel_{III}/AUX compared to Gel_{II}/AUX), while 100% increase in H-bonds led to 51% increase in dissipated energy (Gel_{II}/AUX compared to Gel_{I}/AUX). This proves that the performance of hydrophobic interactions is more significant than internal H-bonds. Furthermore, for the crosslinked microgels a difference was observed between the first and the second loading at the same compression level. During the second cycle, stress-softening occurred and was observed up to the third cycle. For the next cycles no significant softening occurred, which indicates stability of these specimens under load bearing applications.

A frequency sweep analysis (Fig. 5) was performed on AAX/AUX-crosslinked hydrogels. The obtained data showed higher values of G' than G", thus indicating crosslinking of microgels and a dominant elastic behavior [37]. For Gel_{III}/AUX and Gel_{III}/AAX, the presence of reversible physical interactions within the hydrogels resulted in a strong frequency dependence of the measured storage moduli and proved the damping behavior of the hydrogels [38,39]. Additionally, the effect of the reversible interactions within specimens was demonstrated by the elevated G'' values versus frequency [37]. The higher G'' for Gel_{III}/AUX was associated with an increased viscous dissipation ability of the formulations containing AUX linker [38–41]. It is believed that such behavior was observed due to the presence of long flexible PEG400 segments, which increased the viscous component of the specimen due to segmental motion. Most noticeably, both samples showed a nearly sharp increase in G" values beyond frequencies over 50 Hz. This is attributed to the fact that at this frequency, the physical connection between the microgels was destroyed and the damping properties raised abruptly. In the case of Gel_{III}/AAX, G' reached a plateau at frequency over 20 Hz and the cross-over point appeared at 50 Hz, indicating a

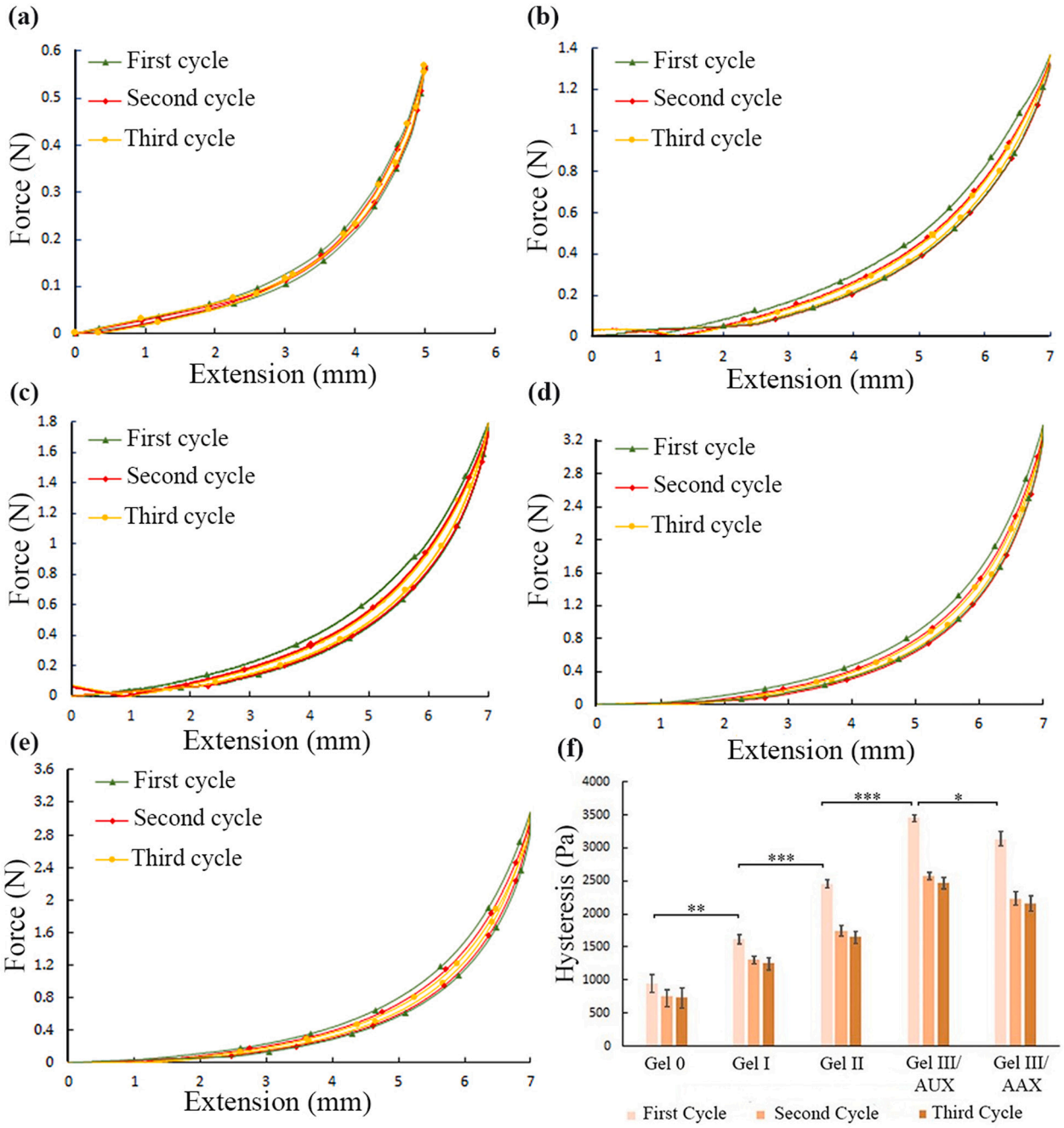

Fig. 4. Cyclic compression loading-unloading curves for Gel_0 (a), Gel_I /AUX (b), Gel_{II} /AUX (c), Gel_{III} /AUX (d) and Gel_{III}/AAX (e). The corresponding dissipated energies of specimens during cyclic loading-unloading test (f).Comparing Gel_{III}/AUX and Gel_{III}/AAX a superior performance of AUX linker to AAX linker was also observed. This is attributed to the ability of flexible hydrophilic PEG segments to move in an aqueous environment, which increases the damping properties of the AUX-crosslinked specimens. For further analysis, rheological properties of specimens formed with these linkers were studied. Error bars represent means ± standard deviation for $n = 4$.

decrease in the elastic character in the gel system arising from network rupture. This may be due to the fact that at a higher frequency region the network structure is no longer intact and the gel matrices break up into smaller units [42]. However, for the AUX-linked specimen, the plateau and cross point occurred over 67 Hz demonstrating a more stable structure than AAX-linked sample.

The GeMs hydrogels are greatly strengthened by applying our strategy compared to previous reports. For Gel_{III} as a typical example, using AUX as elastically effective linker the strength and toughness increased up to 6.8 kPa and 3600 $J.m^{-3}$, respectively (Fig. 6), which is more than 3.5 kPa and 3000 $J.m^{-3}$ for recently reported tough gelatin/alginate hydrogels [43]. As the content of AAc or GMA was increased from Gel_I to Gel_{III}, the fracture energy of hydrogels raised by more than 2 and 3 times, respectively. Moreover, the mechanical properties of Gel_{III} crosslinked via AAX and AUX shows a two-step fracture, which can be attributed to binding of GeMs through both physical and chemical linkages. As particles have the tendency to attach to each other, segregation of clustered network firstly occurred with interruption of physical binding and then the hydrogel broke up completely after chemical bonds disconnection at extension of 81.2% and 89.4% for Gel_{III}/AAX and Gel_{III}/AUX respectively.

Compared to strategies such as self- crosslinking, double networks

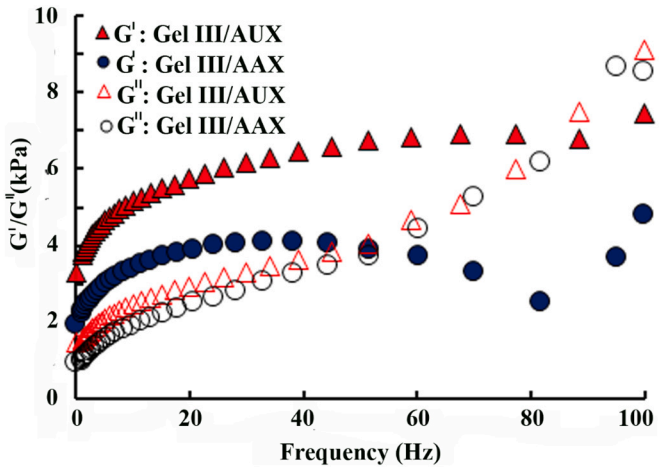

Fig. 5. Storage and loss modulus of GeMs crosslinked with AUX and AAX linkers as a function of frequency.

and inclusion of fillers, we have here applied an effective strategy to fabricate a bulk hydrogel in which microgels play a role as building units. This morphology results in compression strain up to 90% for the Gel_{III}/AUX despite of its higher gelatin content. As summarized in Table 2, the fabricated gelatin hydrogels possess the highest maximum strain and toughness reported till now compared to other strategies for the fabrication of tough gelatin-based hydrogels. It should be noted that those hydrogels with higher compression modulus contain gelatin as the minor component of the network. In this way, the cells will not face a real ECM-like environment. Our strategy used gelatin as the main component with enhanced toughness required for high extension applications such as artificial muscles and mimicking real ECM-like environment.

3.4. Swelling and biodegradability

Super absorbency of hydrogels is one of the most important properties of hydrogels because it has significant influence on physiochemical and mechanical properties [44]. However, fabricating an ultra-high water content gelatin-based hydrogel together with desirable mechanical properties remains still a challenge for a wide spectrum

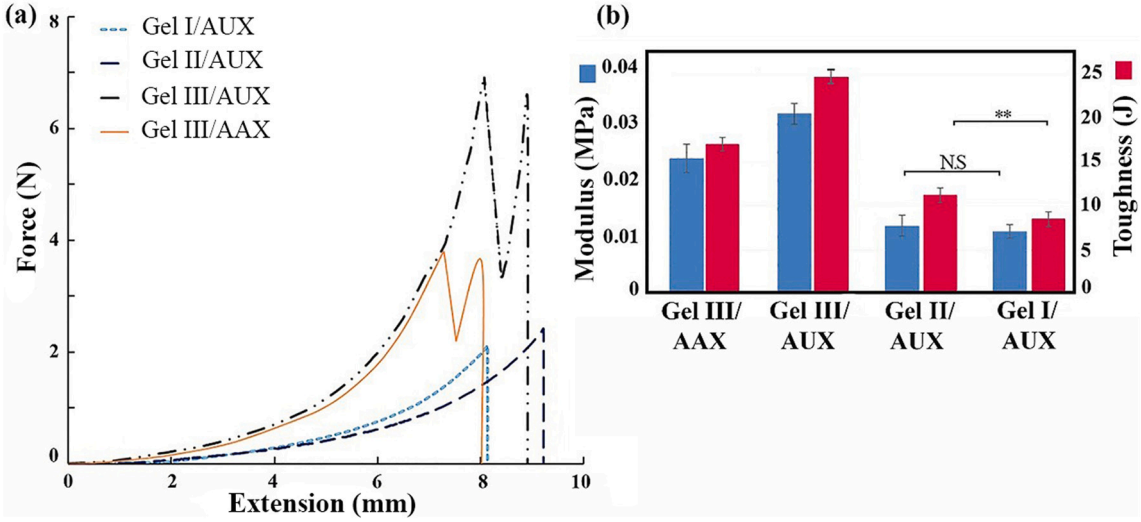

Fig. 6. (a) Force- extension curves of the three types of gels, each compressed to rupture showing a two-step fracture. (b) Modulus and toughness of hydrogels indicates the importance of supramolecular interactions for mechanical properties. Error bars represent means ± standard deviation for $n = 4$. NS = Not Significant. *P*-values are <0.001 for others.

Table 2
A brief comparison of mechanical and physical properties of hydrogels obtained with micro-sized morphology strategy with other methods.

Strategy	Hydrogel components[b]	Percent of gelatin (% *w*/w)	Modulus (kPa)	Max compression strain (%)	Toughness (J/cm^3)	SR (%)	Year	Ref
Self-crosslinking	GTA/hydroxyapatite	70	48.4 MPa	30	1.080± 0.210	–	2010	[19]
	mTG	95<	50	25 >	–	–	2017	[20]
	GTA	95<	150	25 >	–	–	2017	[20]
	GP	95 <	250	25 >	–	–	2017	[20]
	EDC	95 <	51	25 >	–	–	2017	[20]
DN[a]	Alginate/gelatin	15	25	19	–	–	2014	[22]
	Chitosan/gelatin	34	0.73×10^6	64.83	300	500	2013	[24]
	Polyacrylamide /gelatin	10 >	208	64	6.1	–	2018	[28]
	Silk fibroin/gelatin	30 >	600	10	–	93	2019	[63]
Nanocomposite	Clay/gelatin	98	16.5×10^6	25	–	470	2014	[27]
	Graphene oxide /gelatin/ polyacrylamide	10 >	208	47	9.2	30 >	2018	[28]
	N-chitin/gelatin	75 >	31.5×10^6	6.54	–	–	2017	[64]
Microgels	Acrylic acid/glycidyl methacrylate/ gelatin	70 <	30	89	3440	830 <	2020	This work

[a] DN: Double Networks.
[b] Glutaraldehyde (GTA), genipin (GP), 1-ethyl-3-(3-dimethyl aminopropyl)carbodiimide (EDC), and microbial trans glutamin-ase (mTG).

of intrinsically brittle hydrogels including gelatin. Here, we prepared extremely high water content hydrogels driven by specific morphology of the network and a balance between H-bonding and water retention capacity. The effect of different compositions on the swelling behavior of prepared hydrogels was determined (Fig. S6). The swelling ratio increased with increasing AAc concentration from 561 for Gel_I to 854 for Gel_{II}. To our knowledge, this is the highest swelling ratio for gelatin-based hydrogels that has been reported so far (Table 2).

Gelatin is extremely biodegradable due to RGD units. This physiochemical property influences the performance of gelatin-based hydrogels to be used in vivo. However, the method applied here fulfills the requirement and durability of gelatin-based hydrogel. As shown in Fig. S6 (b) the degradation degree of the hydrogels tends to linearly increase with time. The extents of degradation of specimens after 60 days was 70% to complete degradation. Data showed that degradation rate decreased with increasing chemical and physical crosslinking density of hydrogels. In this context Gel_{III}/AUX degraded faster than Gel_{III}/AAX, because AAX possesses more hydrogen bondings than AUX, whereas AUX is more hydrophilic than AAX due to PEG.

The morphology of the hydrogels was well characterized by SEM (Fig. S6(c)). Obtained SEM images exhibited a 3D interconnected pore structure with pores of size 120 ± 35 μm for Gel_{III}/AUX and 95 ± 20 μm for Gel_{III}/AAX. Attachment of GeMs to form multiple particle inter connected associations is completely clear (Fig. S6 (c) in the circle). As mentioned previously, the particles make some entanglements during heating. These entanglements can also be occurred during heating for chemical crosslinking reactions with amine linkers. Another reason for the formation of this porous morphology can be attributed to the crystallization of water molecules during the freezing procedure. Fig. S6 also shows collapsed microgels after freeze drying, which are interconnected.

3.5. Cell viability

The results of MTT assay at days 1, 3 and 7 showed the viability of ASCs in the hydrogels compared to 2D cultures as control (Fig. 7). An increase in proliferation of ASCs on both Gel_{III}/AUX and Gel_{III}/AAX scaffolds at day 3 and 7 compared to 2D control group was observed. However, there were no significant differences between ASCs proliferation in Gel_{III}/AUX and Gel_{III}/AAX scaffolds at day 3 and day 7.

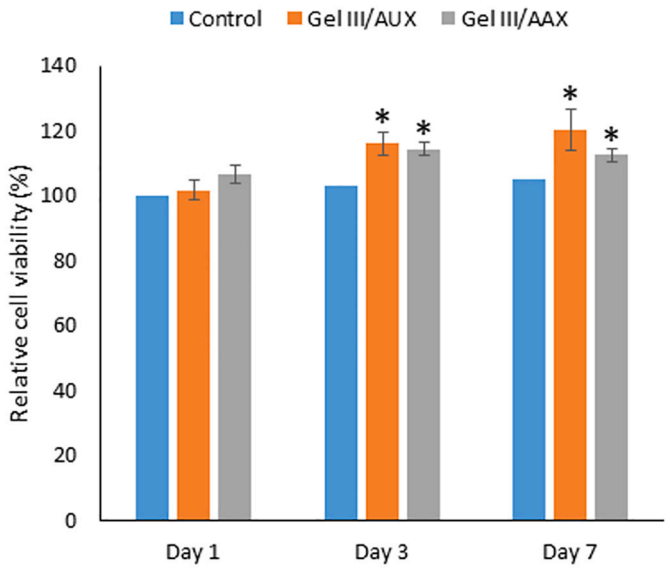

Fig. 7. Relative cell viability for ASCs exposed to Gel $_{III}$/AUX and Gel $_{III}$/AAX scaffolds. (Data presented as mean ± SD, * $p < 0.05$ comparing to control group; $n = 3$.

To further investigate the proliferation of cells seeded on the hydrogels, DAPI staining was used for evaluating cell proliferation in vitro (Fig. S7) [45]. All the cell nuclei stained with DAPI are in blue. The results of DAPI staining showed that the number of cells seeded on the hydrogels increased with culture time. When being cultured for 1 day, the proliferation rate of the cells on both hydrogels was the same as control; however, after 7 days of culture, the proliferation rate of the cells on Gel_{III}/AUX and Gel_{III}/AAX was increased. This may be because of the fact that the seeded cells require more appropriate time to adapt on the first day. On day 7, one can observe a higher number of cells present on Gel_{III}/AUX compared to Gel_{III}/AAX, which is consistent with the results of cytotoxicity analysis.

3.6. In vivo study

In order to evaluate the biocompatibility of the prepared hydrogels in vivo, we investigated their responses in contact with tissue after 4 weeks of implantation. Both Gel_{III}/AUX and Gel_{III}/AAX constructs exhibited a smooth appearance. A thin vascularized capsule was observed surrounding the constructs. Figs. 8 (A) and (B) represent the Gel_{III}/AAX and Gel_{III}/AUX in the implantation site, respectively. After 4 weeks, the scaffolds maintained their integrity, and the inflammation was evidently alleviated. Gel_{III}/AUX scaffolds were degraded in vivo. At time of explanation, a gross morphological examination showed no sign of superficial infection or fistula formation in the implantation site. In addition, the tissue and the scaffolds were easily detached. The response to implantation of the scaffolds at 4 weeks was analyzed by H&E, Masson's trichrome, and toluidine blue staining (Fig. 8). The amount of tissue integration into the implanted hydrogels was assessed using H&E stained sections (Fig. 8 (C) and (D)). Both hydrogels presented some level of tissue integration. The Gel_{III}/AUX hydrogels displayed the least amount of interaction with the surrounding tissue, demonstrating diverse boundaries between the tissue and the hydrogel. In the Gel_{III}/AAX group there was no obvious gap between the implanted scaffold and surrounding tissue (Fig. 8 (C) and (D)). The Gel_{III}/AAX hydrogel showed tissue formations into the hydrogels with more ECM synthesis (Fig. 8 (D)). Also, histological analyses were done to evaluate the presence of different blood cells. Both hydrogels presented a typical infiltration of granulocytes, furthermore macrophages could also be observed at this stage. The Gel_{III}/AAX hydrogel showed a large number of blood vessels compared to Gel_{III}/AUX (Fig. 8, rectangle 1 and 2). At day 28, a moderate inflammatory response was still observed in the hydrogels. However, only very few inflammatory cells could be found in the Gel_{III}/AUX compared to Gel_{III}/AAX hydrogels (Fig. 8, rectangle 1 and 2).

Gelatin-based hydrogels induced the formation of a vascularized tissue within the structure after 4 weeks implantation without incorporation of signaling factors (e.g. vascular endothelial growth factor). Masson's trichrome and toluidine blue staining exhibited new tissue infiltrated in the hydrogels as degradation occurred (Fig. 8-E, F, G and H). The Gel_{III}/AAX hydrogel showed higher collagen deposition into the hydrogels with more ECM synthesis (Fig. 8, rectangle 3 and 4). These observations indicate that our designed hydrogels may be promising for tissue engineering applications.

Even though gelatin is considered to be of high potential for future biomaterials, the brittleness of gelatin constructs is in great contrast with the toughness of biological tissues, which enervate its performance. Thus, we here developed tough hydrogels based on gelatin as their major components by designing micro-sized morphology with locally concentrated dissipation mechanism as an effective strategy in conjunction with preserving water retention capability.

Supramolecular interactions display unique physicochemical properties, such as water-retention capability as well as mechanical properties [46,47], thereby showing great potential in the design and synthesis of supramolecular hydrogels [48,49]. Within the broad scope of supramolecular interactions, a subset of those prepared using

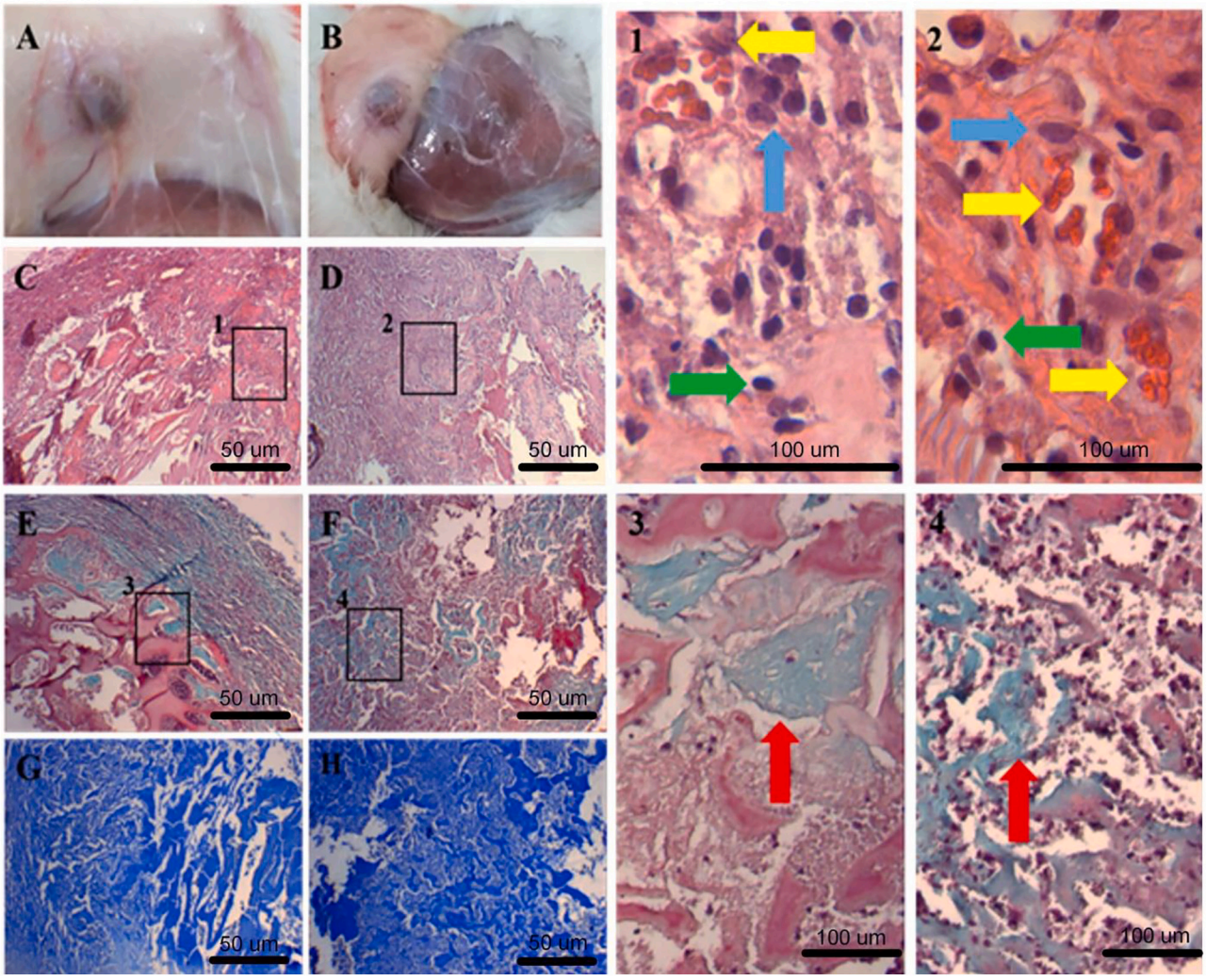

Fig. 8. Scaffolds after 28 days' transplantation in rat. (A) and (B) represents the Gel_{III}/AUX and Gel_{III}/AAX in the implantation site, respectively. Figs. (C), (E), and (G) represent the Gel_{III}/AUX and Figs. (D), (F) and (H) represent the Gel_{III}/AAX for H &E, Masson's trichrome, and Toluidine blue staining after 28 days' implantation, respectively. After 28 days implantation in vivo, all hydrogels showed some level of tissue integration (C and D). General morphology, demonstrating there was obvious formation of the new-tissue around the scaffolds. Arrows shows formation of functional vessels observed after 4 weeks within the scaffolds. The blood vessels, macrophages, and lymphocytes are indicated by the yellow, blue, and green arrows, respectively. The collagen deposition into the hydrogels and ECM synthesis are indicated by the red arrows (Scale bar = 50 μm). (For interpretation of the references to colour in this figure legend, the reader is referred to the web version of this article.)

hydrogen bond and hydrophobic interactions are of considerable interest. As illustrated in literature polymers carrying H-bonding sites offer required elasticity due to inter-chain exchange and bond reformation [50–54]. Concentration levels and the strength of H-bonds are the main factors determining mechanical strength and network elasticity offering variable dynamic behavior [50]. According to a similar mechanism of energy dissipation, for instance, in the system designed by Wang et al. strong multiple hydrogen bonds formed between poly(vinyl alcohol) (PVA) and tannic acid (TA) molecules, acted as permanent crosslinks, while weaker hydrogen bonds between PVA chains acted as reversible crosslinks [55]. Hydrophobic interactions, as another type of supramolecular interactions, can play a critical role in a wide range of molecular assembling [56,57]. To increase the toughness of hydrogels through supramolecular interactions, the system must contain hydrophobic groups to associate and form crosslinked points [58–60]. This strategy can be applied, for example, through copolymerizing hydrophilic and hydrophobic monomers in a micellar solution. However, the resulting hydrogels have limited water absorbance capability [61,62]. Here, we tried to apply a synthesis strategy to fabricate hydrogels through which water absorption and energy dissipation are located in separate sectors, so that they couldn't interfere. We hypothesized that high concentration of supramolecular interactions in micro-sized domains as toughening mechanism could effectively render energy dissipation near the crack point.

Compared to strategies such as self-crosslinking, double networks, macromolecular microsphere composite hydrogels and inclusion of fillers, in this work a micro-sized dissipative morphology strategy was used to separate dissipating energy and water absorption sites. The remarkable enhancement in mechanical properties of crosslinked GeMs hydrogels is attributed to the coagulation of GeMs particles due to the presence of dissociable physical interaction between GeMs as well as breakage of H-bonds present into the GeMs; however, it was found that the performance of hydrophobic interactions of PGMAs was more significant since such interactions get ruptured on loading, resulting in separation and sliding of GeMs following damping of applied energy.

4. Conclusion

The methodology that we have here developed and entitled micro-sized morphology with locally concentrated dissipation mechanism

can be considered as an effective strategy in conjunction with preserving water retention capability. It should be noted that the performance of the methodology introduced here is comparable to strategies such as double crosslinking, inter-penetrating networks and incorporation of fillers, and can be applied to wide spectrum of polymers whose practical application requires efficient toughness. Thus, it is expected that the procedure reported here introduces a sustainable method for the preparation of extensible hydrogels, which suffer from brittle nature especially in the presence of large water content. Finally, these hydrogels are expected to be promising candidates for future biomedical applications thanks to their in vitro and in vivo biocompatibility results.

CRediT authorship contribution statement

Author	Contribution
Mehdi Sheikhi	Conceptualization, Methodology, Investigation, Writing, Formal analysis, Validation, Software
Fatemeh Rafiemanzelat	Corresponding author, supervision, Project administration, Data curation, Funding acquisition, Validation; resources, Visualization, review and editing, Software
Lorenzo Moroni	Corresponding author, supervision, Visualization, Data curation, review and editing
Mohsen Setayeshmehr	Methodology, Project administration, Visualization, Data curation, Validation; resources, review and editing

Declaration of competing interest

The authors declare that they have no known competing financial interests or personal relationships that could have appeared to influence the work reported in this paper.

Acknowledgements

The authors would like to acknowledge for supporting this work from office of vice chancellor for research and technology of university of Isfahan.

Appendix A. Supplementary data

Supplementary data to this article can be found online at https://doi.org/10.1016/j.msec.2020.111750.

References

[1] M. Spang, C. Karen, Extracellular matrix hydrogel therapies: in vivo applications and development, Acta Biomater. 68 (2018) 1–14.
[2] M. Setayeshmehr, E. Esfandiari, B. Hashemibeni, A. Tavakoli, M. Rafienia, A. Samadikuchaksaraei, L. Moroni, M. Joghataei, Chondrogenesis of human adipose-derived mesenchymal stromal cells on the [devitalized costal cartilage matrix/poly (vinyl alcohol)/fibrin] hybrid scaffolds, Eur. Polym 118 (2019) 528–541.
[3] S. Santhanam, Y. Shui, J. Struckhoff, B. Karakocak, P.D. Hamilton, G.J. Harocopos, N. Ravi, Bioinspired fibrillary hydrogel with controlled swelling behavior: applicability as an artificial vitreous, ACS Appl. Bio Mater. 2 (2018) 70–80.
[4] V. Keskar, M. Gandhi, E.J. Gemeinhart, R.A. Gemeinhart, Initial evaluation of vascular ingrowth into superporous hydrogels, J. Tissue Eng. Regen. M. 3 (2009) 486–490.
[5] M. Köllmer, V. Keskar, T.G. Hauk, J.M. Collins, B. Russell, R.A. Gemeinhart, Stem cell-derived extracellular matrix enables survival and multilineage differentiation within superporous hydrogels, Biomacromolecules 13 (2012) 963–973.
[6] M. Setayeshmehr, E. Esfandiari, M. Rafieinia, B. Hashemibeni, A. Taheri-Kafrani, A. Samadikuchaksaraei, D.L. Kaplan, L. Moroni, M.T. Joghataei, Hybrid and composite scaffolds based on extracellular matrices for cartilage tissue engineering, Tissue Eng. Part B Rev 25 (2019) 202–224.
[7] D. Lee, J. E. Choi, S. E. Lee, K. L. Kang, H. J. Moon, H. J. Kim, Y. S. Hwang, Injectable biodegradable gelatin-methacrylate/β-tricalcium phosphate composite for the repair of bone defects. Chem. Eng. J. 365 (2019)30–39.
[8] S. Afewerki, A. Sheikhi, S. Kannan, S. Ahadian, A. Khademhosseini, Gelatin-polysaccharide composite scaffolds for 3D cell culture and tissue engineering: towards natural therapeutics, Bioengineering. Transla. Med 4 (2019) 96–115.
[9] W. Huang, D. Restrepo, J.Y. Jung, F.Y. Su, Z. Liu, R.O. Ritchie, J. McKittrick, P. Zavattieri, D. Kisailus, Multiscale toughening mechanisms in biological materials and bioinspired designs, Adv. Mater. 31 (2019) 1901561.
[10] Y. Alinejad, A. Adoungotchodo, E. Hui, F. Zehtabi, S. Lerouge, An injectable chitosan/chondroitin sulfate hydrogel with tunable mechanical properties for cell therapy/tissue engineering, Int. J. Biol. Macromol. 113 (2018) 132–141.
[11] H. Luo, Y. Zhang, Z. Wang, Z. Yang, J. Tu, Z. Liu, F. Yao, G. Xiong, Yizao Wan, Constructing three-dimensional nanofibrous bioglass/gelatin nanocomposite scaffold for enhanced mechanical and biological performance, Chem. Eng. J. 326 (2017) 210–221.
[12] M. Azami, M. Rabiee, F. Moztarzadeh, Glutaraldehyde crosslinked gelatin/hydroxyapatite nanocomposite scaffold, engineered via compound techniques, Polym 31 (2010) 2112–2120.
[13] G. Yang, Z. Xiao, H. Long, K. Ma, J. Zhang, X. Ren, J. Zhang, Assessment of the characteristics and biocompatibility of gelatin sponge scaffolds prepared by various crosslinking methods, Sci. Rep. 8 (2018) 1–13.
[14] S. Farris, J. Song, Q. Huang, Alternative reaction mechanism for the cross-linking of gelatin with glutaraldehyde, J. Agric. Food Chem. 58 (2010) 998–1003.
[15] B. Sarker, D.G. Papageorgiou, R. Silva, T. Zehnder, F. Gul-E-Noor, M. Bertmer, J. Kaschta, K. Chrissafis, R. Detsch, A.R. Boccaccini, Fabrication of alginate–gelatin crosslinked hydrogel microcapsules and evaluation of the microstructure and physico-chemical properties, J. Mater. Chem. B 2 (2014) 1470–1482.
[16] B. Balakrishnan, N. Joshi, A. Jayakrishnan, R. Banerjee, Self-crosslinked oxidized alginate/gelatin hydrogel as injectable, adhesive biomimetic scaffolds for cartilage regeneration, Acta Biomater. 10 (2014) 3650–3663.
[17] Z. Shen, X. Cui, R. Hou, Q. Li, H. Deng, J. Fu, Tough biodegradable chitosan–gelatin hydrogels via in situ precipitation for potential cartilage tissue engineering, RSC Adv. 569 (2015) 55640–55647.
[18] J.L. Vanderhooft, M. Alcoutlabi, J.J. Magda, G.D. Prestwich, Rheological properties of cross-linked hyaluronan–gelatin hydrogels for tissue engineering, Macromol. Biosci. 9 (2009) 20–28.
[19] X. Wang, Q. Ao, X. Tian, J. Fan, H. Tong, W. Hou, S. Bai, Gelatin-based hydrogels for organ 3D bioprinting, Polymers 9 (2017) 401.
[20] A. Farahnaky, S.M.M. Dadfar, M. Shahbazi, Physical and mechanical properties of gelatin–clay nanocomposite, J. Food Eng. 122 (2014) 78–83.
[21] X. Yan, J. Yang, F. Chen, L. Zhu, Z. Tang, G. Qin, Qiang Chen, G. Chen, Mechanical properties of gelatin/polyacrylamide/graphene oxide nanocomposite double-network hydrogels, Comos, Sci. Technol. 163 (2018) 81–88.
[22] R.E. Webber, C. Creton, H.R. Brown, J.P. Gong, Large strain hysteresis and Mullins effect of tough double-network hydrogels, Macromolecules 40 (2007) 2919–2927.
[23] D.C. Tuncaboylu, M. Sari, W. Oppermann, O. Okay, Tough and self-healing hydrogels formed via hydrophobic interactions, Macromolecules 44 (2011) 4997–5005.
[24] A. Ahagon, A.N. Gent, Threshold fracture energies for elastomers, J. Polym. Sci. B Polym. Phys. 13 (1975) 1903–1911.
[25] L.B. Jiang, D.H. Su, S.L. Ding, Q.C. Zhang, Z.F. Li, F.C. Chen, W. Ding, S.T. Zhang, J. Dong, Salt-assisted toughening of protein hydrogel with controlled degradation for bone regeneration, Adv. Funct. Mater. 29 (2019) 1901314.
[26] R. Long, C.Y. Hui, Fracture toughness of hydrogels: measurement and interpretation, Soft Matter 12 (2016) 8069–8086.
[27] A.M. Costa, J.F. Mano, Extremely strong and tough hydrogels as prospective candidates for tissue repair–a review, Eur. Polym. J. 72 (2015) 344–364.
[28] O. Okay, S. Durmaz, Charge density dependence of elastic modulus of strong polyelectrolyte hydrogels, Polymer 43 (2002) 1215–1221.
[29] C. Li, C. Mu, W. Lin, Novel hemocompatible nanocomposite hydrogels crosslinked with methacrylated gelatin, RSC Adv. 6 (2016) 43663–43671.
[30] Z. He, Y. Wang, T. Zhao, Z. Ye, H. Huang, Ultrasonication-assisted rapid determination of epoxide values in polymer mixtures containing epoxy resin, Anal. Methods 6 (2014) 4257–4261.
[31] E. Hoch, C. Schuh, T. Hirth, G.E. Tovar, K. Borchers, Stiff gelatin hydrogels can be photo-chemically synthesized from low viscous gelatin solutions using molecularly functionalized gelatin with a high degree of methacrylation, J. Mater. Sci. Mater. Med. 23 (2012) 2607–2617.
[32] T. Billiet, B. V. Gasse, E. Gevaert, M. Cornelissen, J. C. Martins, P. Dubruel, Quantitative contrasts in the photopolymerization of acrylamide and methacrylamide-f unctionalized gelatin hydrogel building blocks, Macromol. Biosci. 13 (2013) 1531–1545.
[33] S.H. Ching, N. Bansal, B. Bhandari, Rheology of emulsion-filled alginate microgel suspensions, Food Res. Int. 80 (2016) 50–60.
[34] I.F. Farrés, M. Douaire, I.T. Norton, Rheology and tribological properties of Ca-alginate fluid gels produced by diffusion-controlled method, Food Hydrocoll. 32 (2013) 115–122.
[35] P.N. Charron, T.A. Braddish, R.A. Oldinski, PVA-gelatin hydrogels formed using combined theta-gel and cryo-gel fabrication techniques, J. Mech. Behav. Biomed. Mater. 92 (2019) 90–96.
[36] A.M. Kristen, M.A. Grunlan, Modern strategies to achieve tissue-mimetic, mechanically robust hydrogels, ACS Macro Lett. 8 (2019) 705–713.
[37] J. Mangelschots, M. Bibian, J. Gardiner, L. Waddington, Y.V. Wanseele, A. V. Eeckhaut, M.M. Diaz Acevedo, et al., Mixed α/β-peptides as a class of short amphipathic peptide hydrogelators with enhanced proteolytic stability, Biomacromolecules 17 (2016) 437–445.
[38] K.C. Bentz, N. Sultan, D.A. Savin, Quantitative relationship between cavitation and shear rheology, Soft Matter 14 (2018) 8395–8400.
[39] Y. Li, H. Meng, Y. Liu, A. Narkar, B.P. Lee, Gelatin microgel incorporated poly (ethylene glycol)-based bioadhesive with enhanced adhesive property and bioactivity, ACS Appl. Mater. Interfaces 8 (2016) 11980–11989.

[40] X. Ding, G.K. Vegesna, H. Meng, A. Winter, B.P. Lee, Nitro-group functionalization of dopamine and its contribution to the viscoelastic properties of catechol-containing nanocomposite hydrogels, Macromol. Chem. Phys. 216 (2015) 1109–1119.
[41] B.P. Lee, M.H. Lin, A. Narkar, S. Konst, R. Wilharm, Modulating the movement of hydrogel actuator based on catechol–iron ion coordination chemistry, Sensor Actuat B-Chem 206 (2015) 456–462.
[42] S. Samai, C. Sapsanis, S.P. Patil, A. Ezzeddine, B.A.M. Hesham Omran, A. Emwas, K.N. Salama, N.M. Khashab, A light responsive two-component supramolecular hydrogel: a sensitive platform for the fabrication of humidity sensors, Soft Matter 12 (2016) 2842–2845.
[43] M.A. Samp, N.C. Iovanac, A.J. Nolte, Sodium alginate toughening of gelatin hydrogels, ACS. Biomater. Sci. Eng. 3 (2017) 3176–3182.
[44] A. Suzuki, S. Sasaki, Swelling and mechanical properties of physically crosslinked poly (vinyl alcohol) hydrogels, J. Eng. Med. 229 (2015) 828–844.
[45] H. Afjoul, A. Shamloo, A. Kamali, Freeze-gelled alginate/gelatin scaffolds for wound healing applications: an in vitro, in vivo study, Mater. Sci. Eng. C 110957 (2020).
[46] R. Dong, Y. Pang, Y. Su, X. Zhu, Supramolecular hydrogels: synthesis, properties and their biomedical applications, Biomater. Sci 3 (2015) 937–954.
[47] X.H. Wang, F. Song, D. Qian, Y.D. He, W.C. Nie, X.L. Wang, Y.Z. Wang, Strong and tough fully physically crosslinked double network hydrogels with tunable mechanics and high self-healing performance, Chem. Eng. J. 349 (2018) 588–594.
[48] J. Hoque, N. Sangaj, S. Varghese, Stimuli-responsive supramolecular hydrogels and their applications in regenerative medicine, Macromol. Biosci. 19 (2019) 1800259.
[49] H. Wang, L. Chen, L. Fang, L. Li, J. Fang, C. Lu, Z. Xu, Supramolecular hydrogel hybrids having high mechanical property, photoluminescence and light-induced shape deformation capability: design, preparation and characterization, Mater Design 160 (2018) 194–202.
[50] Y. Yang, X. Ding, M.W. Urban, Chemical and physical aspects of self-healing materials, Prog. Polym. Sci. 49 (2015) 34–59.
[51] Y. Chen, A.M. Kushner, G.A. Williams, Z. Guan, Multiphase design of autonomic self-healing thermoplastic elastomers, Nat. Chem. 4 (2012) 467.
[52] P. Cordier, F. Tournilhac, C. Soulié-Ziakovic, L. Leibler, Self-healing and thermoreversible rubber from supramolecular assembly, Nature 451 (2008) 977–980.
[53] F. Herbst, S. Seiffert, W.H. Binder, Dynamic supramolecular poly (isobutylene) s for self-healing materials, Polym. Chem. 3 (2012) 3084–3092.
[54] G.M. van Gemert, J.W. Peeters, S.H. Söntjens, H.M. Janssen, A.W. Bosman, Self-healing supramolecular polymers in action, Macromol. Chem. Phys. 213 (2012) 234–242.
[55] Y.N. Chen, L. Peng, T. Liu, Y. Wang, S. Shi, H. Wang, Poly (vinyl alcohol)–tannic acid hydrogels with excellent mechanical properties and shape memory behaviors, ACS Appl. Mater. Interfaces 8 (2016) 27199–27206.
[56] J. Fox, J.J. Wie, B.W. Greenland, S. Burattini, W. Hayes, H.M. Colquhoun, M. E. Mackay, S.J. Rowan, High-strength, healable, supramolecular polymer nanocomposites, J. Am. Chem. Soc. 134 (2012) 5362–5368.
[57] P.J. Woodward, D.H. Merino, B.W. Greenland, I.W. Hamley, Z. Light, A.T. Slark, W. Hayes, Hydrogen bonded supramolecular elastomers: correlating hydrogen bonding strength with morphology and rheology, Macromolecules 43 (2010) 2512–2517.
[58] M. Mihajlovic, M. Staropoli, M.S. Appavou, H.M. Wyss, W. Pyckhout-Hintzen, R. P. Sijbesma, Tough supramolecular hydrogel based on strong hydrophobic interactions in a multiblock segmented copolymer, Macromolecules 50 (2017) 3333–3346.
[59] Y. Deng, I. Hussain, M. Kang, K. Li, F. Yao, S. Liu, G. Fu, Self-recoverable and mechanical-reinforced hydrogel based on hydrophobic interaction with self-healable and conductive properties, Chem. Eng. 353 (2018) 900–910.
[60] X.N. Zhang, Y.J. Wang, S. Sun, L. Hou, P. Wu, Z.L. Wu, Q. Zheng, A tough and stiff hydrogel with tunable water content and mechanical properties based on the synergistic effect of hydrogen bonding and hydrophobic interaction, Macromolecules 51 (2018) 8136–8146.
[61] F. Yang, B. Ren, Y. Cai, J. Tang, D. Li, T. Wang, Z. Feng, Y. Chang, L. Xu, J. Zheng, Mechanically tough and recoverable hydrogels via dual physical crosslinkings, J. Polym. Sci. Polym. Phys. 56 (2018) 1294–1305.
[62] M. Pekař, Hydrogels with micellar hydrophobic (nano) domains, Front Mater 1 (2015) 35.
[63] W. Xiao, J. Li, X. Qu, L. Wang, Y. Tan, K. Li, H. Li, X. Yue, B. Li, X. Liao, Cell-laden interpenetrating network hydrogels formed from methacrylated gelatin and silk fibroin via a combination of sonication and photocrosslinking approaches, Mater. Sci. Eng. 99 (2019) 57–67.
[64] S. Sahraee, J.M. Milani, B. Ghanbarzadeh, H. Hamishehkar, Physicochemical and antifungal properties of bio-nanocomposite film based on gelatin-chitin nanoparticles, Int. J. Biol. Macromol. 97 (2017) 373–381.

Update

Materials Science & Engineering C

Volume 126, Issue , July 2021, Page

DOI: https://doi.org/10.1016/j.msec.2021.112133

Materials Science & Engineering C 126 (2021) 112133

Contents lists available at ScienceDirect

Materials Science & Engineering C

journal homepage: www.elsevier.com/locate/msec

Corrigendum

Corrigendum to "Ultrahigh-water-content biocompatible gelatin-based hydrogels: Toughened through micro-sized dissipative morphology as an effective strategy" [Mater. Sci. Eng. C 120 (2021) 111750]

M. Sheikhi [a], F. Rafiemanzelat [a,*], L. Moroni [b,*], M. Setayeshmehr [b,c,d]

[a] Polymer Chemistry Research Laboratory, Department of Chemistry, University of Isfahan, Isfahan 81746-73441, Islamic Republic of Iran
[b] MERLN Institute for Technology Inspired Regenerative Medicine, Complex Tissue Regeneration Department, Maastricht University, Universiteitssingel 40, 6229ER Maastricht, the Netherlands
[c] Department of Biomaterials, Tissue Engineering and Nanotechnology, School of Advanced Technologies in Medicine, Isfahan University of Medical Sciences, Isfahan, Iran
[d] Department of Tissue Engineering & Regenerative Medicine, Faculty of Advanced Technologies in Medicine, Iran University of Medical Sciences (IUMS), Tehran, Iran

The authors regret to have made a mistake on their published article in one of the affiliations as well as corresponding authors details.

The correct affiliation "a" should be [a] Polymer Chemistry Research Laboratory, Department of Chemistry, University of Isfahan, Isfahan 81746-73441, Islamic Republic of Iran.

And the corresponding author details should be:

Corresponding authors at: [a] Polymer Chemistry Research Laboratory, Department of Chemistry, University of Isfahan, Isfahan 81746-73441, Islamic Republic of Iran.

[b] MERLN Institute for Technology Inspired Regenerative Medicine, Complex Tissue Regeneration Department, Maastricht University, Universiteitssingel 40, 6229ER Maastricht, the Netherlands.

E-mail addresses: frafiemanzelat@chem.ui.ac.ir (F. Rafiemanzelat), l.moroni@maastrichtuniversity.nl (L. Moroni).

The authors would like to apologise for any inconvenience caused.

DOI of original article: https://doi.org/10.1016/j.msec.2020.111750.
* Corresponding authors.
E-mail addresses: frafiemanzelat@chem.ui.ac.ir (F. Rafiemanzelat), l.moroni@maastrichtuniversity.nl (L. Moroni).

https://doi.org/10.1016/j.msec.2021.112133

Available online 12 May 2021